

Oscillations of Thick Accretion Discs Around Black Holes – II

Eduardo Rubio-Herrera ^{*} and William H. Lee

Instituto de Astronomía, UNAM, Apartado Postal 70–264 C.P. 04510 México D.F. México.

Released 2005 Xxxxx XX

ABSTRACT

We present a numerical study of the global modes of oscillation of thick accretion discs around black holes. We have previously studied the case of constant distributions of specific angular momentum. In this second paper, we investigate (i) how the size of the disc affects the oscillation eigenfrequencies, and (ii) the effect of power-law distributions of angular momentum on the oscillations. In particular, we compare the oscillations of the disc with the epicyclic eigenfrequencies of a test particle with different angular momentum distributions orbiting around the central object. We find that there is a frequency shift away from the epicyclic eigenfrequency of the test particle to lower values as the size of the tori is increased. We have also studied the response of a thick accretion disc to a localized external perturbation using non constant specific angular momentum distributions within the disc. We find that in this case it is also possible (as reported previously for constant angular momentum distributions) to efficiently excite internal modes of oscillation. In fact we show here that the local perturbations excite global oscillations (acoustic p modes) closely related to the epicyclic oscillations of test particles. Our results are particularly relevant in the context of low mass X-ray binaries and microquasars, and the high frequency Quasi-Periodic Oscillations (QPOs) observed in them. Our computations make use of a Smooth Particle Hydrodynamics (SPH) code in azimuthal symmetry, and use a gravitational potential that mimics the effects of strong gravity.

Key words: accretion discs — black hole physics — hydrodynamics — stars: neutron — X-rays: binaries

1 INTRODUCTION

Thick accretion discs may appear in systems containing compact objects such as black holes and neutron stars. These could form in different scenarios governed by gravitational forces. Specific examples are: (i) gravitational collapse of a rotating massive star, (ii) the coalescence of two compact objects or (iii) accretion phenomena associated with Low Mass X-ray Binaries (LMXBs).

The first case (gravitational collapse), may be related to the production of γ -ray bursts (GRBs) as in the collapsar or hypernova models. The collapsar (or failed supernova) was proposed by Woosley (1993) and offers the possibility to form a thick disc when the mantle of a rotating massive star ($M \sim 25M_{\odot}$) falls freely onto the recently formed black hole. The material has a very high angular momentum, which prevents it from directly accreting and a centrifugally supported disc is formed. These systems are related to energetic, long

duration (> 2 s) GRBs accompanied by a Type Ib/Ic supernova (Kulkarni et al. 1998; Stanek et al. 2003; Hjorth et al. 2003). Similar numerical relativistic calculations concerning the collapse of massive stars, reported by Shapiro & Shibata (2002) and Shibata & Shapiro (2002) may explain the formation of massive black holes surrounded by a debris torus. The hypernova scenario was proposed by Paczyński (1998) and is also related to GRBs. Hypernovæ are extremely energetic supernova explosions (*kinetic energy* $\sim 3 \times 10^{52}$ erg), which consider (a) a single star (i.e. Wolf-Rayet type star) or (b) a binary system formed by massive stars ($M \sim 20 - 25M_{\odot}$) orbiting closely ($\sim 1.5R_{\odot}$) around each other, and which eventually merge to form a single star [see Nomoto, Maeda, Mazzali, Umeda, Deng & Iwamoto (2004) for a comprehensive review]. This star will undergo gravitational collapse, leading to the formation of a compact object. Due to the rapid rotation, a thick accretion disc around the remaining black hole will be formed. In either case, a hot, thick disc of $\sim 0.1M_{\odot}$ is expected around the newborn black hole.

^{*} E-mail: eduardo@astroscu.unam.mx

Another possibility to form thick discs is via the coalescence of two compact objects, leading to the formation of a system composed of a black hole and an accretion torus. This has been investigated by various groups using numerical simulations. Some of the first results were obtained by Davies, Benz, Piran & Thielemann (1994), who modeled the merger of two neutron stars. They showed that after few orbital periods the residual material could form a thick disc. These results have been confirmed and extended (see e.g., Ruffert, Janka & Schäfer 1996; Ruffert & Janka 1999) for the merger of two neutron stars, where again, a hot thick disc is formed around a central mass, which will presumably collapse to a black hole. Investigating the more complex fusion of a neutron star and a black hole, Kluźniak & Lee (1998) and Lee (2001) found that after the initial mass transfer there is a remnant of material around the black hole (see also recent results by Rosswog, Speith & Wynn 2004). All these scenarios may form massive ($M_d/M_{BH} \approx 0.1$) and dense discs.

There are also low-mass discs ($M_d/M_{BH} \ll 1$) which are formed through mass transfer in a binary system. A steady supply of mass, energy and angular momentum produces structures which are nearly in a steady state, but which nevertheless exhibit variability on various timescales (see e.g., Kato 1998).

Once the disc is formed, one may ask: under which conditions is it dynamically stable or unstable (quite apart from the question of thermal stability, if dynamically stable)? Answering this in any detail requires the consideration of viscosity, self-gravity, magnetic fields and the angular momentum distribution of the material within the disc. This last point led Papaloizou & Pringle (1984) to investigate the stability of an isentropic and constant angular momentum disc, and find that it is unstable to global non-axisymmetric perturbations. Three-dimensional calculations by Zurek & Benz (1986) found that there is indeed a redistribution of angular momentum within the disc, due to the growth of non-axisymmetric instabilities. In the presence of accretion, however, this instability may be suppressed (Blaes 1987), and thick tori with relatively flat distributions of angular momentum may actually occur in astrophysical systems.

Perhaps one of the most interesting global instabilities is the so-called runaway radial instability, which was identified by Abramowicz, Calvani & Nobili (1983). It is due to a violent mass exchange associated with the rapidly changing equipotential Roche surfaces of the disc + black hole system. It is catastrophic and leads to the complete destruction of the disc on a dynamical time scale. It is well known that in binary systems there is a point called the interior Lagrangian point L_1 , located at a radius r_{L_1} where there is a balance between gravitational and centrifugal forces. For accreting discs, when mass transfer from the disc to the central object begins the corresponding Lagrange point, lying between the compact object and the disc, moves outward. The accretion rate increases rapidly until the disc is accreted completely. Wilson (1984) found that the rotation of the black hole inhibits the runaway radial instability and later Abramowicz, Karas & Lanza (1998) confirmed this result and reported that the self-gravity of the disc has a destabilizing effect. It appears that the most critical parameter in the runaway radial instability

is the specific angular momentum distribution within the disc. In the last twenty five years there has been much work on this issue from *stationary* (i.e. Schwarzschild metric) to *dynamical* (i.e. Kerr metric) space-time models. A complete summary of the work done appears in the extensive work of Font & Daigne (2002) and Daigne & Font (2004). These authors conclude, as Daigne & Mochkovitch (1997) did earlier, that the instability is suppressed when the angular momentum follows a power law distribution with a positive radial gradient. In this respect studies made by Ruffert & Janka (1999) and Lee (2001) concerning compact binary mergers show that the distribution of angular momentum in post-merger discs is far from being constant, and thus they are stable in this context.

Our numerical simulations were performed in order to address two questions: (i) How do thick discs oscillate? and (ii) How does a localized perturbation affect the global oscillatory behaviour of the disc? These are formulated in the particular context in the millisecond oscillations discovered in X-ray binary sources by *RXTE* (van der Klis 2000). These systems have compact objects surrounded by an accretion disc, whose variability could be imprinted on the X-ray lightcurve and corresponding power spectra.

Disc oscillations have been investigated numerically and analytically by several groups before, and may be applied to the quasi periodical oscillations (QPOs) observed in many X-ray sources (Perez et al. 1997; Wagoner 1999; Silbergleit et al. 1999; Ortega-Rodríguez et al. 2002). One specific model (Rezzolla, Yoshida, Maccarone & Zanotti 2003a) accounts for the high frequency QPOs as a result of p-mode oscillations of an accretion torus orbiting close to the black hole. Rezzolla, Yoshida & Zanotti (2003b) investigated theoretically how a relativistic torus oscillates in a stationary Schwarzschild space-time, showing that the eigenfrequencies of the axisymmetric oscillations correspond to acoustic p-modes. Their results shows that the oscillations behaves like a sound wave globally trapped within the disc, with the eigenfrequencies appearing in the sequence 2:3:4... independently of the distribution of angular momentum considered. The same conclusions are obtained by Zanotti, Font, Rezzolla & Montero (2005) using numerical simulations for a dynamical Kerr space-time, concluding that p-mode oscillations in relativistic tori could explain the high frequency QPOs observed in the X-ray binaries. The oscillatory analysis made by Rezzolla et al. (2003a), Rezzolla et al. (2003b), Montero et al. (2004) and Zanotti et al. (2005) has shown theoretically that there is a frequency shifting to lower frequencies as the size of the torus is increased. Their analytical work is restricted to height-integrated structures and globally applied perturbations. We have confirmed this result more generally here with a different approach.

From the observations in the X-ray band mentioned above, Abramowicz & Kluźniak (2001) noted in GRO J1655–40, that the two stable peaks that appear in the power spectrum in the hHz range are in a 3:2 ratio. The same commensurability has now been observed in three more sources: H1743–322, XTE J1550–564 and GRS 1915+105 (see McClintock & Remillard 2004, for a recent review). This behaviour may also be present in a system containing a neutron star (Sco X–1) (Abramowicz, Bulik, Bursa & Kluźniak 2003), and could be explained by parametric resonance

in a thin disc (Abramowicz et al. 2003; Rebusco 2004). These models predict that the frequencies will show the epicyclic motions of a perturbed flow line in the accretion disc or a combination of these and a fixed perturbation associated to the spin of the central object (in the neutron star sources). This last issue was analysed by Kluźniak et al. (2004), Lee, Abramowicz & Kluźniak (2004) and Rubio-Herrera & Lee (2005, hereafter Paper I) showing that it is indeed possible to excite internal oscillatory modes efficiently by an external driving agent.

In this paper we show that there is a shifting to lower frequencies as the thickness of the disc is increased, independently of the distribution of angular momentum within the torus. We also show that it is possible to excite internal p-modes in a thick accretion disc, by means of a localized perturbation which affects only a small portion of the disc periodically, exciting the strongest modes apparent in a 3:2 frequency ratio.

We emphasize that the results presented here are purely dynamical in a pseudo-Newtonian gravitational potential which mimics the properties of the Schwarzschild metric for a stationary space-time. No attempt has been made to consider magnetic fields, radiation or the effects of viscosity. For definiteness, a numerical value of $2.5M_\odot$ has been used throughout the paper. The reader should keep in mind, though, that distances are always measured in units of the gravitational radius. As such, our results are scale free, and can be applied to any black hole mass, with the frequencies scaling as $\nu \propto 1/M$.

2 INITIAL CONDITIONS AND NUMERICAL METHOD

2.1 Hydrostatic equilibrium for a thick torus

We will define a thick torus as that which has similar radial and vertical extensions, i.e., $L \sim H$, and where L is comparable to its radial position, R . We will neglect self-gravity and additionally assume azimuthal symmetry. We have constructed thick tori using the pseudo-Newtonian gravitational potential proposed by Paczyński & Wiita (1980), given by:

$$\Phi = \frac{-GM_{BH}}{R - r_g}, \quad (1)$$

which qualitatively reproduces the behaviour of a test particle in the Schwarzschild metric, and accounts correctly for the positions of the marginally stable and marginally bound orbits. In this equation, $R = \sqrt{r^2 + z^2}$ is the radial distance measured from the central mass and $r_g = 2GM_{BH}/c^2$ denotes the Schwarzschild radius of the central object. Using a polytropic equation of state $P = K\rho^\gamma$, the equations of hydrodynamics in cylindrical coordinates, and neglecting self gravity, we have:

$$\frac{1}{\rho} \nabla P = -\nabla \Phi_{\text{eff}} \quad (2)$$

where Φ_{eff} is the effective potential. Using the Paczyński-Wiita expression given in (1), substituting it in (2) and integrating over r we have,

$$\frac{\gamma}{\gamma - 1} \frac{P}{\rho} + \Phi_{\text{eff}} + \Phi_0 = \text{cst}, \quad (3)$$

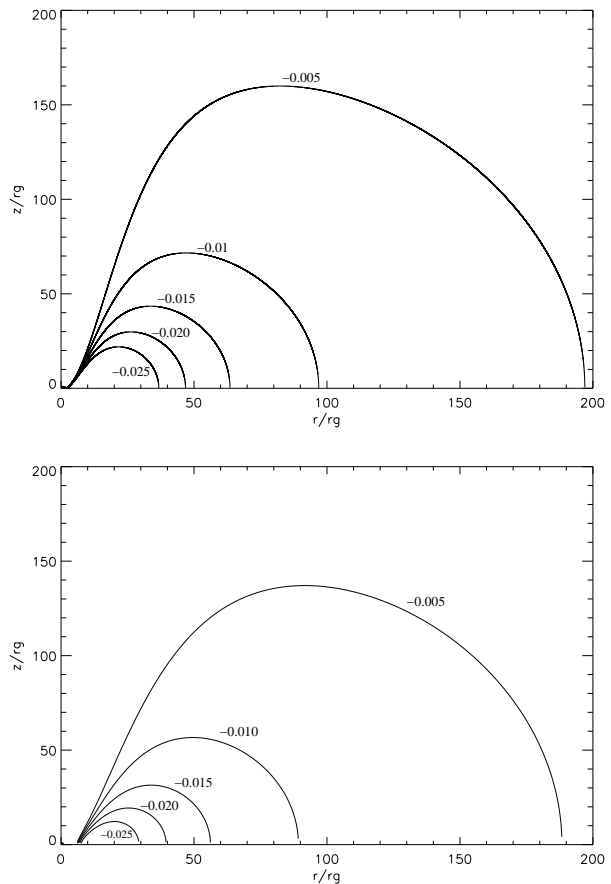


Figure 1. Meridional cross-sections over one half the r - z plane for tori with constant specific angular momentum, $\ell = \text{const}$ (above), and a power-law specific angular momentum distribution $\ell \propto r^\alpha$, $\alpha = 0.1$ (bottom). The filling factor Φ_0 is indicated in units of $c^2/2$.

which describes a torus in hydrostatic equilibrium. The term Φ_0 can be interpreted as a filling factor of the effective potential well, and will be discussed below. Using an arbitrary distribution of angular momentum $\ell(r)$, which depends only of the position coordinate r according to the von Zeipel theorem for a polytropic equation of state, the effective potential takes the form:

$$\Phi_{\text{eff}} = \frac{-GM_{BH}}{R - r_g} + \int \frac{\ell(r')^2}{2r'^3} dr'. \quad (4)$$

The boundary of the torus is the surface over which the pressure is zero, and is given by:

$$z = \left\{ \left[GM_{BH} \left(\int \frac{\ell(r')^2}{2r'^3} + \Phi_0 \right)^{-1} + r_g \right]^2 - r^2 \right\}^{1/2}. \quad (5)$$

The corresponding meridional cross sections over one half the r - z plane are shown in Figure 1 for various filling factors Φ_0 and different distributions of specific angular momentum. Several groups have studied the dynamics and stability of tori with varying distributions of specific angular momentum (Daigne & Font 2004; Font & Daigne 2002; Masuda, Nishida & Eriguchi 1998; Daigne & Mochkovitch 1997). In summary, the conclusion has been that in a torus

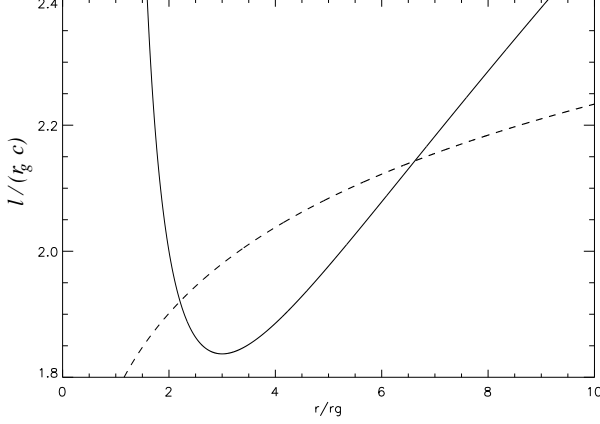


Figure 2. Angular momentum distributions used for our models. The solid line represents a Keplerian angular momentum distribution for test particles in circular orbits, while the dashed line shows the non-constant power law distribution. For the case with uniform angular momentum we used $\ell = 1.92 r_g c$.

with non-constant angular momentum, the runaway radial instability is suppressed. We have performed calculations (described below) in this context, and have used the value $\ell = 1.92 r_g c$ for a constant distribution. This corresponds to the angular momentum of a test particle in a Keplerian motion at $r = 4.25 r_g$. For the power law distribution case we used

$$\ell(r) = \ell_K \left(\frac{r}{r_0} \right)^\alpha, \quad (6)$$

where

$$\ell_K = \left(r^3 \frac{\partial \Phi_e}{\partial r} \right)_{r=r_0}^{1/2} = \left[\frac{GM_{BH} r^3}{(r - r_g)^2} \right]_{r=r_0}^{1/2}. \quad (7)$$

The value of the power index α , can be super-keplerian $\alpha > 0.5$, keplerian $\alpha = 0.5$ or sub-keplerian $\alpha < 0.5$. To compare with the results obtained by Font & Daigne (2002), we have used a sub-keplerian distribution with an index $\alpha = 0.1$. Finally the normalizing factor for the radius is that which corresponds to the Keplerian value $r_0 = 5.1 r_g$. We will henceforth define the centre of the torus as the locus (a circle, really) of maximum density and pressure in the disc.

2.2 Numerical method

We have used the SPH (Smooth Particle Hydrodynamics) numerical method to perform our simulations (Monaghan 1992). Essentially this method works by interpolating a desired function $A(r)$, with a set of given quantities $A(r')$ through a *kernel* function $W(r, h)$, using the following convolution integral:

$$A(r) = \int A(r') W(r - r') dr. \quad (8)$$

The implementation of the code was made using the prescriptions calculated by Monaghan & Lattanzio (1985) when the system has azimuthal symmetry, using the following *kernel* function:

$$W(r, h) = \frac{\sigma}{h^\nu} \begin{cases} 1 - 3(r/h)^2/2 + 3(r/h)^3/4 & \text{if } 0 \leq r/h \leq 1; \\ (2 - r/h)^3/4 & \text{if } 1 \leq r/h \leq 2; \\ 0 & 2 \leq r/h. \end{cases} \quad (9)$$

In the last equation, h represents the smoothing length, and is comparable to the typical separation between fluid elements, and r is the radial coordinate (h is essentially the spatial resolution of the calculation). As our calculations were performed in two dimensions, $\nu = 2$ and $\sigma = 10/7\pi$. We did not include the viscosity of the gas and hence the Navier–Stokes equations of motion take the form:

$$\frac{dv_r}{dt} = -\frac{1}{\rho} \frac{\partial P}{\partial r} - \frac{GM_{BH} r}{R(R - r_g)^2} + r\Omega^2 + \left(\frac{dv_r}{dt} \right)_{art}, \quad (10)$$

$$\frac{dv_z}{dt} = -\frac{1}{\rho} \frac{\partial P}{\partial z} - \frac{GM_{BH} z}{R(R - r_g)^2} + \left(\frac{dv_z}{dt} \right)_{art}, \quad (11)$$

where again $R = \sqrt{r^2 + z^2}$ is the distance to the central object. The sub-index *art* indicates the artificial viscosity terms, used in the numerical calculations to account for the presence of shocks and avoid particle interpenetration. We have additionally for the conservation of angular momentum:

$$\frac{d\ell}{dt} = 0. \quad (12)$$

And finally, for the energy equation we have:

$$\frac{d\epsilon}{dt} = - \left(\frac{P}{\rho} \right) \nabla \cdot \vec{v} + \left(T \frac{ds}{dt} \right)_{art} \quad (13)$$

where ϵ is the internal energy per unit mass. We have assumed that we do not have losses of energy by external causes (i.e. $\Delta Q = 0$) and the only changes in ϵ arise from mechanical work done on the system. In discretized form for numerical work, the convolution integral given in equation (8) becomes a sum over all the fluid elements in the calculation.

For the artificial viscosity, we have used the prescription given by Balsara (1995) which reduces the artificial shearing stress during the time evolution of the disc. The explicit forms for the acceleration and the energy dissipation due to artificial viscosity for the i -*eth* SPH particle are then:

$$\left(\frac{d\vec{v}}{dt} \right)_{i,art} = - \sum_{j \neq i} m_j \Pi_{ij} \nabla_i W_{ij}, \quad (14)$$

and

$$\left(T \frac{ds}{dt} \right)_{i,art} = \frac{1}{2} \sum_{j \neq i} m_j \Pi_{ij} (\vec{v}_i - \vec{v}_j) \cdot \nabla_i W_{ij}. \quad (15)$$

where, again, W is the *kernel* function and Π is defined by (see e.g., Lee & Ramirez-Ruiz 2002)

$$\Pi_{ij} = \left(\frac{P_i}{\rho_i^2} + \frac{P_j}{\rho_j^2} \right) = (-\alpha_b \mu_{ij} + \beta_b \mu_{ij}^2), \quad (16)$$

$$\mu_{ij} = \begin{cases} \frac{(\vec{v}_i - \vec{v}_j) \cdot (\vec{r}_i - \vec{r}_j)}{h_{ij} (|\vec{r}_i - \vec{r}_j|^2 / h_{ij}^2 + \eta^2)} - \frac{(f_i + f_j)}{2c_{ij}} & \text{if } (\vec{v}_i - \vec{v}_j) \cdot (\vec{r}_i - \vec{r}_j) < 0; \\ 0 & \text{if } (\vec{v}_i - \vec{v}_j) \cdot (\vec{r}_i - \vec{r}_j) \geq 0; \end{cases} \quad (17)$$

In this last equation the function f_i is defined by:

$$f_i = \frac{|\nabla \cdot \vec{v}|_i}{|\nabla \cdot \vec{v}|_i + |\nabla \times \vec{v}|_i + \eta' c_i / h_i}. \quad (18)$$

The factor $\eta' \simeq 10^{-4}$ in the denominator prevents numerical divergences, c_i represents the sound speed and h_i is the

length scale for the i -th particle. $\alpha_b = \beta_b = \gamma/2$ are constants of order unity and γ is the polytropic index from the equation of state. This form of the artificial viscosity suppresses the shearing stresses when the compression in the fluid is low and the vorticity is high $|\nabla \cdot \vec{v}| \ll |\nabla \times \vec{v}|$, but remains in effect if the compression dominates in the flow $|\nabla \cdot \vec{v}| \gg |\nabla \times \vec{v}|$.

2.3 Initial conditions

Our initial conditions are generated by fixing the mass of the central object, the equation of state, with $\gamma = 4/3$ and the constant K , the filling factor for the potential, Φ_0 and the distribution of angular momentum $\ell(r)$. We then generate the fluid elements which will model the torus using a Monte Carlo random number generator. The particles that fall inside the torus density profile will be the fluid elements of the simulation. These fluid elements are then relaxed for several dynamical times with an artificial damping term included in the equations of motion in order to obtain the a distribution which is as close to equilibrium as possible. We are able to build tori of different sizes by simply varying the filling factor Φ_0 as was shown in Figure 1.

Our initial configurations are always non-accreting tori, confined inside their Roche lobe, i.e., $r_{in} > r_{L1}$ where r_{in} is the distance from the central object to the inner edge of the torus and r_{L1} is the radius of the inner Lagrange point, L_1 . When we focus on the pure oscillation dynamics of the disc, we also wish to avoid accretion. In those cases, this is accomplished by maintaining the mass of the black hole constant (even if some particles overflow the Roche lobe as a result of the applied perturbation).

Our code produces different snapshots of the main hydrodynamical variables of the system like the position of the centre of the disc, and also the maximum and mean densities and the potential, kinetic and internal energies as functions of time. This data then is analysed by calculating the corresponding Fourier transforms and looking for characteristic frequencies.

2.4 Testing the code

To test our code, we performed simulations reproducing previously published results (Abramowicz, Calvani & Nobili (1983), Daigne & Mochkovitch (1997), Abramowicz, Karas & Lanza (1998), Font & Daigne (2002) and Daigne & Font (2004)) investigating the behavior of the runaway-radial instability with changing distributions of angular momentum (in systems without self-gravity). We constructed tori that (i) almost fill their effective potential wells, i.e., $r_{in} \simeq r_{L1}$, and (ii) have constant and non constant angular momentum distributions. We then introduced radial impulsive perturbations, adding a velocity field to the initial distribution. This field is similar to the solution proposed by Michel (1972) for spherical relativistic accretion, and has the form

$$\begin{aligned} \vec{v}_r &= -\eta \cdot \sqrt{r_g/R} \hat{r}, \\ \vec{v}_z &= -\eta \cdot \sqrt{r_g/R} \hat{z}, \end{aligned} \quad (19)$$

where the parameter $\eta \ll 1$ modulates the strength of the perturbation.

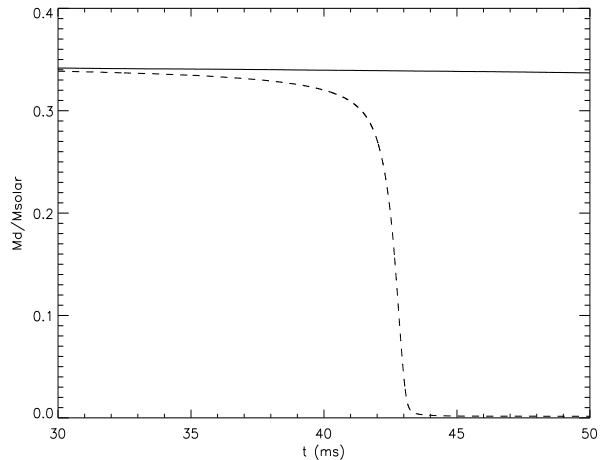


Figure 3. Mass in the disc as a function of time for two test runs. The dashed line corresponds to the model with constant angular momentum distribution within the disc ($\ell = \text{cst}$), while the solid line corresponds to the model with a power law angular momentum distribution $\ell \propto r^\alpha$.

We have found results that are in complete agreement with the previous work available in the literature, that is, the runaway instability is completely suppressed when one considers a non-constant angular momentum distribution within the torus. This is shown in Figure 3, where the mass of the disc is plotted as a function of time for a calculation with a power law distribution of specific angular momentum (solid line), and another with constant specific angular momentum (dashed line). The former is clearly stable, while the latter is not, and shows the characteristic runaway behavior. Once the instability is triggered, the torus is destroyed in a few dynamical times.

3 NATURAL OSCILLATIONS OF THE DISC

To study the free oscillations of the disc, we have performed calculations where small, impulsive perturbations have been applied to the velocity field, as in equation (19), only in the initial conditions. This was done in particular to study how the thickness of the disc affects its modes of oscillation. The space-time around the black hole was kept constant during this set of runs, even if slight overflow occurred through the inner Lagrange point.

3.1 Epicyclic frequencies

The results obtained were compared with the behaviour of a test particle in a circular orbit around a central mass. If we introduce a small radial perturbation, the particle will show radial oscillations at the epicyclic frequency κ . Our study begins with the equation for radial motion of the particle:

$$\frac{d^2 r}{dt^2} = -\frac{d\Phi_{\text{eff}}}{dr}. \quad (20)$$

Introducing a perturbation of the form: $\Delta r = r - r_0$, and calculating a first order Taylor expansion over r for small perturbations, we obtain

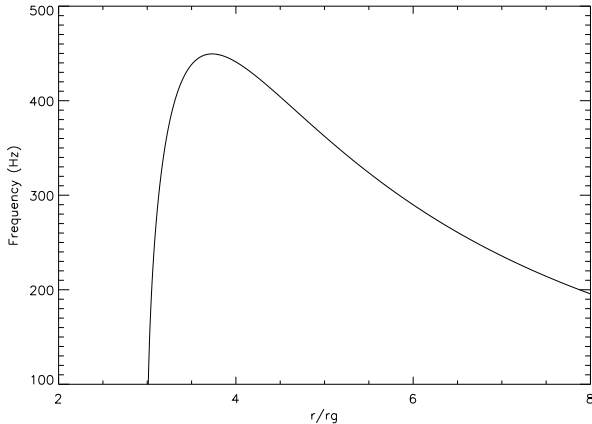


Figure 4. Epicyclic frequency κ as a function of radius. The curve is computed for a test particle orbiting a central object of $2.5M_{\odot}$. Compare with Figures 5 and 6.

$$\frac{d^2 \Delta r}{dt^2} = - \left(\frac{d^2 \Phi_{\text{eff}}}{dr^2} \right)_0 \Delta r, \quad (21)$$

for a fixed radius. This equation is simply that of a harmonic oscillator, with epicyclic frequency $\kappa = (d^2 \Phi_{\text{eff}}/dr^2)_0^{1/2}$. For a constant angular momentum ($\ell = \text{cst}$), we have:

$$\kappa(r) = \frac{1}{2\pi} \sqrt{\frac{GM_{BH}(r - 3r_g)}{r(r - r_g)^3}}. \quad (22)$$

In Figure 4 we show the radial dependency of $\kappa(r)$.

3.2 Results

We show here results for tori of three different sizes: small ($r_d < r_g$), intermediate ($r_d \sim r_g$) and large ($r_d > r_g$), both for $\ell = \text{cst}$ and $\ell(r) = r^\alpha$. In each case we computed the Fourier transform of the radial motions of the centre of the disc. This always exhibited one prominent peak, at frequency κ^* . In the limit of small tori, $\kappa^* \rightarrow \kappa(r_0)$, the value for test particle motion. As the size of the torus increases, there is a shift to lower frequencies, and κ^* decreases. The Fourier transforms and the corresponding values for the frequencies (along with the model parameters) are given in Figures 5 and 6, and in Table 1. These numerical results agree with the work reported by Rezzolla, Yoshida, Maccarone & Zanotti (2003a) and by Rezzolla, Yoshida & Zanotti (2003b), where the frequency shift has been computed analytically in the Schwarzschild metric (albeit with the aforementioned simplification of height-integrated equations). We thus confirm the p-mode interpretation of Rezzolla et al. (2003), in which *the radial epicyclic frequency at the position of the centre of the torus represents the value at which the fundamental p-mode frequency tends to in the limit of vanishing torus size.*

4 LOCALIZED PERIODIC PERTURBATIONS AND GLOBAL RESPONSE

4.1 A localized external perturbation

Having identified the strongest response in the radial oscillations as a modified epicyclic frequency, or p-mode, we proceeded to apply localized, periodic perturbations to thick tori (as in Paper I). We believe it is reasonable to assume that the perturbation will be stronger in the inner regions of the disc, if it arises from the central object, and periodic, if it is related to its spin period (clearly identifiable in neutron star systems) or some other mechanism repeating at intervals $\Delta t = 1/\nu_{\text{per}}$. This perturbation can be related to a wide variety of phenomena coming from the central object or from the material that conforms the disc. A specific example could be the emission of gravitational radiation from the black hole when a clump of material is accreted and breaks the axial symmetry in a quasi-periodic fashion. This could produce a time variation in the mass quadrupole of the disc itself (Zanotti, Rezzolla & Font 2003). Another possibility in this context was proposed by van Putten (2001), and is related to the connection between the magnetic field of the disc and the gravitational radiation produced by the black hole. Disc oscillations can be related to the formation of the disc, or to its intrinsic properties. Simulations by Igumenshchev, Chen & Abramowicz (1996) have shown that variability and oscillations can be triggered by viscous processes. Kato (2001) has suggested that energy flux within the disc through viscous and angular momentum processes can alter the equilibrium state, producing oscillations. Finally, in highly dynamical situations, the disc will naturally lack complete azimuthal symmetry (e.g., in compact object mergers) and the formation of clumps inside the disc could lead to small oscillations.

We have modeled perturbations in the context of non-constant angular momentum discs in the same way that we did in Paper I, introducing an additional acceleration in the equations of motion, given by:

$$a_{\text{pert}} = -\eta a_g \cdot \exp\left(\frac{r_0 - r}{\delta r}\right) \cdot \sin(2\pi\nu_{\text{pert}}t). \quad (23)$$

Here a_g is the acceleration due to gravity, r_0 is the outer edge of the torus and $\eta \ll 1$ is a parameter that modulates the strength of the perturbation. The exponential term decays on a scale $\delta r \simeq R$, the radial extension of the disc, thus reproducing the desired behaviour for the perturbative force, which will be strong near the inner radius and weak in the outer regions. This acceleration induces radial oscillations, which can be Fourier analyzed to extract the main frequencies in a similar fashion as was done by Lee, Abramowicz & Kluźniak (2004).

4.2 Results

We performed simulations using constant and non-constant angular momentum distributions within the disc. For the constant distribution, we find, as described in Paper I for a few particular cases, that the localized perturbation induces global oscillations at various characteristic frequencies. The most prominent (besides that occurring at the perturbing frequency ν_{per}) is at $\nu_1 = \kappa^*$, the modified epicyclic frequency associated with the radial motions of the centre of the disc.

Table 1. Models for discs of different size orbiting a $2.5M_\odot$ black hole. We give the extent of the disc r_d , the disc to black hole mass ratio (M_d/M_{BH}), the angular momentum value ($\ell_0/r_g c$) or distribution ($\ell \propto r^\nu$), the locus of the point of maximum density (R_c/r_g), the filling factor which gives us the size of the torus ($\Phi_0/(c^2/2)$), the eigenfrequency κ^* at which the point of maximum density oscillates, and the number of SPH particles we used in the simulation (N).

Model	size (r_d)	M_d/M_{BH}	$\ell_0/r_g c$	R_c/r_g	$\Phi_0/(c^2/2)$	κ^* (Hz)	N
(a)	$r_d < r_g$	3.0×10^{-8}	1.9197	4.25	-0.1183	425	2337
(b)	$r_d \sim r_g$	5.9×10^{-3}	1.9197	4.25	-0.1060	355	2886
(c)	$r_d > r_g$	0.14	1.9197	4.25	-0.0841	290	4082
(d)	$r_d < r_g$	1.6×10^{-8}	$\propto r^\nu$	5.10	-0.0749	350	2317
(e)	$r_d \sim r_g$	2.0×10^{-3}	$\propto r^\nu$	5.10	-0.0678	300	1866
(f)	$r_d > r_g$	0.3	$\propto r^\nu$	5.10	-0.0595	250	1630

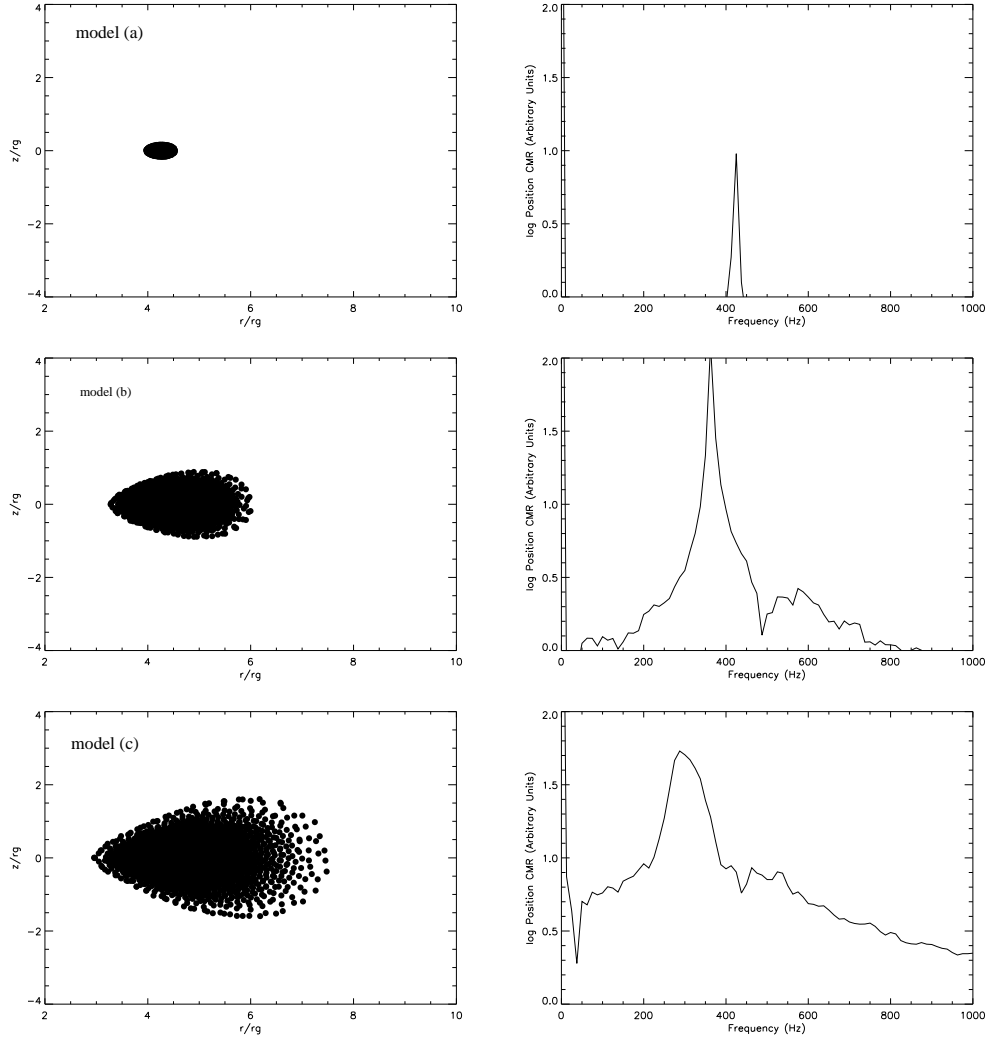


Figure 5. Meridional cross sections for a small, intermediate and large torus (left panels), for a constant angular momentum distribution ($\ell = \text{cst}$), and Fourier transforms of the radial oscillations of the centre of the torus for each case (hereafter represented by the letters CMR in the figures) in the right panels. The discs orbit a $2.5M_\odot$ black hole. Note how the eigenfrequency κ^* is progressively shifted to lower values as the size of the torus increases and compare with the epicyclic eigenfrequency for a test particle shown in Figure 4. For all the unperturbed tori shown here, the centre is located at $r = 4.25r_g$.

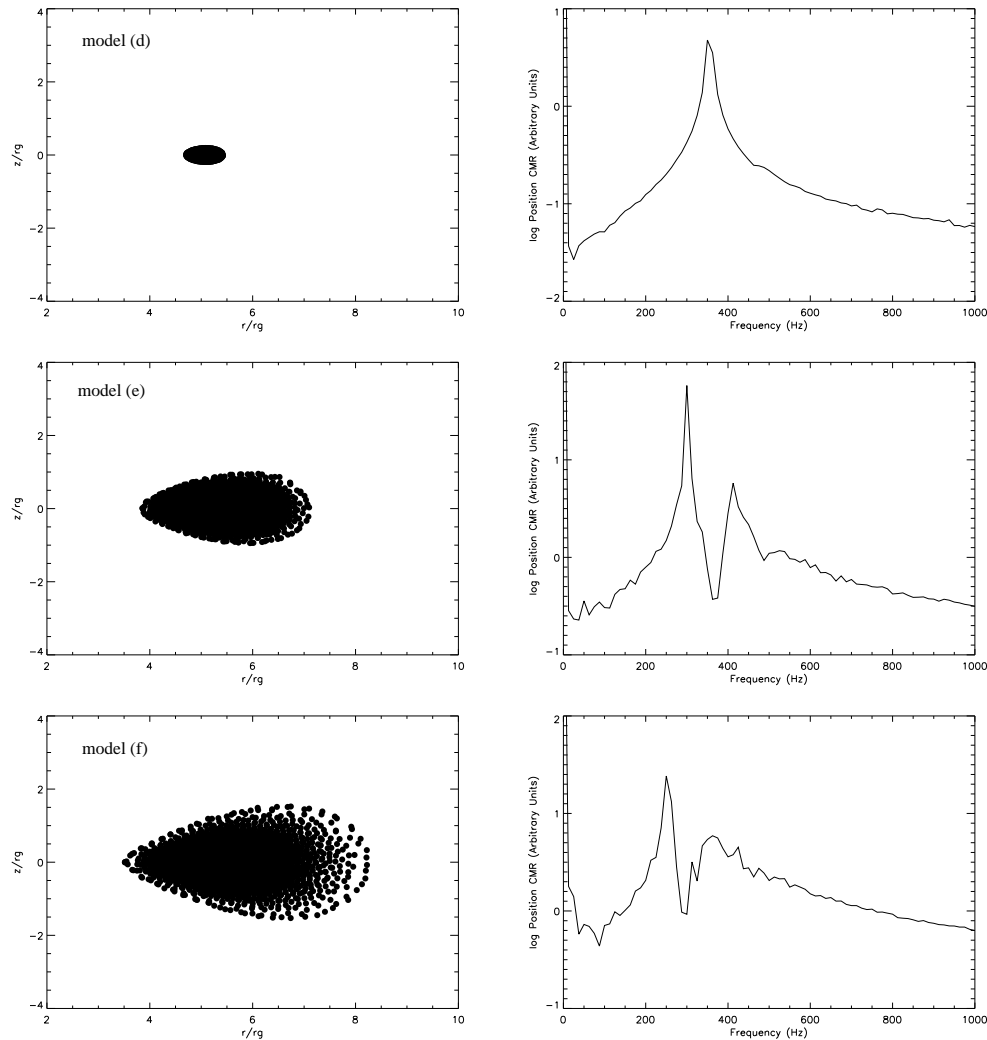


Figure 6. Same as Figure 5, but for a power-law angular momentum distribution ($\ell \propto r^\alpha$). For all the unperturbed tori shown here, the centre is located at $r = 5.1r_g$.

A second broad peak with about ten times less power at ν_2 is in a 3:2 relation with the former (see Figure 7). This latter feature is barely made out in the calculations where an impulsive perturbation was applied to the whole disc at $t = 0$.

For a power law distribution of angular momentum we find that the disc responds somewhat differently to the localized perturbation. A typical power spectrum for the radial motions of the centre of the disc is shown in Figure 8 (when $\nu_{per} = 100$ Hz). Two strong narrow peaks are evident at ν_{per} and $2\nu_{per}$, despite the fact that the perturbation is a pure sinusoid. Furthermore, a weak subharmonic at $\nu_{per}/2$ is also present. This is clear evidence of non-linear coupling between various modes, and is reminiscent of analogous results for forced oscillations in slender tori previously reported in the context of kHz QPOs in LMXBs (Lee, Abramowicz & Kluźniak 2004). Note that the overtone is absent in the power spectrum in Figure 7 (when the angular momentum is constant in the disc). As for the case with constant angular momentum, two more peaks, at $\nu_1 = \kappa^* = 250$ Hz, and $\nu_2 \approx 1.5\nu_1$ can be seen in the

spectrum. To the limit of our resolution, they are in a 3:2 correspondence. Thus it appears that the angular momentum distribution is somehow responsible for a certain mode coupling which allows higher harmonics and subharmonics of the perturbation to appear in the power spectrum. Note also that when an impulsive perturbation was used in a thick torus with a power law distribution of angular momentum, secondary features, consistent with being in a 3:2 relation with the stronger ones, are apparent in the spectrum once the torus becomes relatively thick (see Figure 6, middle and bottom right panels). Apparently the periodic nature of the forcing also has a direct influence on the magnitude of the response of the system. We elaborate further on this point below in § 5.

5 DISCUSSION

We have performed a numerical study of the global oscillations of geometrically thick fluid tori in axisymmetry. We have neglected self-gravity, but used a pseudo-potential to

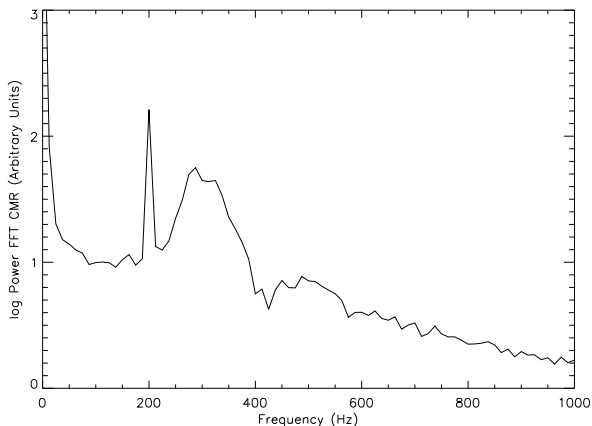


Figure 7. Fourier power spectrum for the radial oscillations of the centre of a torus (CMR) with a constant angular momentum distribution, when perturbed periodically. Three main peaks are apparent. From left to right, the first one is the oscillation induced at $\nu_{per} = 200$ Hz, the second is the modified epicyclic frequency (p-mode) at $\nu_1 = \kappa^* = 300$ Hz, and the third is in a 3:2 relation with κ^* , at frequency $\nu_2 = 450$ Hz.

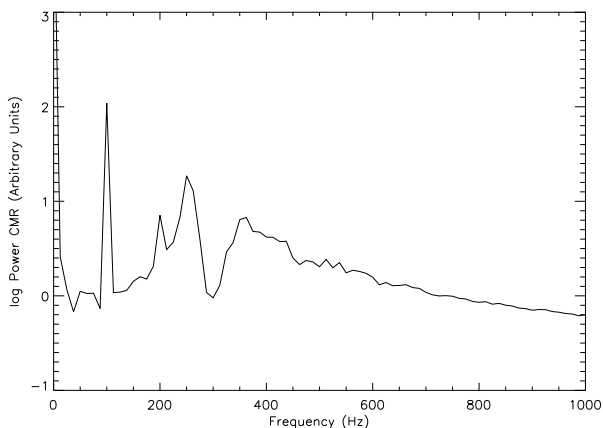


Figure 8. Fourier power spectrum for the radial oscillations of the centre of a torus (CMR) with a power law distribution of angular momentum, $\ell(r) \propto r^\alpha$, when perturbed periodically. Several peaks are apparent. The strongest one is at the perturbation frequency, $\nu_{per} = 100$ Hz. A harmonic at 200 Hz and a weak subharmonic at 50 Hz are also visible. The fundamental p-mode is at $\nu_1 = \kappa^* = 250$ Hz, and the weaker first overtone at $\nu_2 = 360$ Hz. The latter two are approximately in a 3:2 ratio.

mimic the effects of strong gravity for the potential produced by the central mass. After building initial conditions in hydrostatic equilibrium with a prescribed rotation law (given through the distribution of specific angular momentum within the disc), global impulsive and localized periodic perturbations have been applied, and the disc's response has been measured through the time variation of certain quantities, and their corresponding Fourier transforms. An ideal gas equation of state has been used throughout.

As the size of the torus is increased by filling up the effective potential well to a greater degree (see Figures 1, 5 and 6), we find, by applying impulsive kicks, that the fun-

damental global mode of radial oscillations monotonically decreases from the analytic expression for the local radial epicyclic frequency at the position of the centre of the torus. This effect is present independently of the assumed distribution of angular momentum (be it a constant or a power law). That is, a slender torus tends to oscillate as a free particle would, and a thicker one does so at lower frequencies. This effect is simply due to the increased size of the resonant cavity, and the density stratification within it which affects the propagation of sound waves. It was found analytically in calculations performed in the Schwarzschild metric with height-integrated tori for inertial-acoustic modes (p-modes) recently (Rezzolla, Yoshida, Maccarone & Zanotti 2003a; Rezzolla, Yoshida & Zanotti 2003b), and we confirm it here for the more general case of a full torus perturbed slightly from equilibrium.

Upon application of a localized and periodic external perturbation, however, the torus responds in a manner which does depend on the distribution of angular momentum. As previously reported in the context of LMXBs (Paper I), for $\ell = \text{cst}$ the fundamental radial mode at frequency κ^* and the first overtone at $1.5\kappa^*$ are excited (although the overtone is noticeably weaker than the fundamental).

For a power law distribution of angular momentum (specifically we used $\ell(r) \propto r^{0.1}$), the fundamental at κ^* was always present, as was the first overtone at $\approx 1.5\kappa^*$. Furthermore, a harmonic of the perturbation itself, at $2\nu_{per}$, and a subharmonic at $\nu_{per}/2$ always appeared. We take this latter fact to indicate the presence of non-linear mode coupling, since the applied perturbation was purely sinusoidal and contained only a single frequency.

Trial calculations in both cases revealed that varying the perturbation frequency ν_{per} by a factor of a few had no discernible effect on the results (i.e., this is not the result of a coincidence of fundamental frequencies and overtones with the particular choice for the perturbation frequency).

Similar results concerning the relative amplitudes of various modes when $\ell(r)$ is varied can actually be extracted from the study of Rezzolla and collaborators. In particular, Figure 3 in (Rezzolla, Yoshida & Zanotti 2003b) shows the response (in the density) of a torus with constant angular momentum when given an impulsive perturbation. The first overtone is weaker than the fundamental by a factor of $\simeq 30$. However, results for tori with power-law distributions in $\ell(r)$ show a much larger contrast, with the fundamental and its harmonics dominating the frequency spectrum, and p-mode overtones being much weaker (about three orders of magnitude, see Figure 4 in Zanotti, Font, Rezzolla & Montero (2005)). To complicate matters, it would appear that the way in which the perturbation is applied (e.g., only in the density vs. only in the velocity, or both) has an important effect on the amplitude of the response (see Figure 5 in Zanotti, Font, Rezzolla & Montero (2005)). In calculating the eigenfunctions for the height-integrated problem, Rezzolla and collaborators have found that these become vanishingly small near the inner edge of the torus in certain cases, thus making these modes harder to excite. In all cases, and as one would expect, they report that the most efficient way to excite oscillations is to use a perturbation which matches the corresponding eigenfunction (i.e., this is when the strongest response occurs). We have only attempted one type of perturbation here, given in equation (25), and so

have not explored this effect. The vanishing of the eigenfunction may explain formally why certain oscillations are suppressed, or equivalently, why they are so hard to excite with arbitrary perturbations.

In the context of QPOs in LMXBs, producing variability in the X-ray lightcurve from the oscillations described here is beyond the scope of this work (see e.g., Schnittman 2005, for how this may actually come about). However, if it is actually related to the QPOs, one could argue that the presence of definite frequencies, and their relation to one another, may serve as an indicator of the distribution of angular momentum within the disc, or of its relative thickness.

We believe the study presented here captures the essentials of the simple system at hand, namely, one with pure hydrodynamics in the field of a central object, neglecting self gravity and assuming azimuthal symmetry. Clearly in a real astrophysical situation these conditions will not be strictly met. Magnetic fields are likely to play an important role and make the system more complex by introducing additional possible modes, as well as coupling to the hydrodynamics. Even without magnetic fields, the tori described here will not be isolated in a vacuum, but surrounded by a gaseous envelope, the rest of the disk. Mode coupling and/or leakage at the interface is likely to affect the oscillatory behaviour of the system and is a consideration that deserves further study (for a preliminary study addressing these matters see Fragile 2005).

ACKNOWLEDGMENTS

We gratefully acknowledge helpful discussions with M. A. Abramowicz, W. Kluźniak and L. Rezzolla. This work was supported in part by CONACyT (36632E).

REFERENCES

- Abramowicz M. A., Calvani M., Nobili L. 1983, *ApJ*, 242, 772
- Abramowicz M. A., Karas, V., Lanza, A. 1998, *A&A*, 331, 1143
- Abramowicz M. A., Kluźniak W. 2001 *A&A*, 374, L19
- Abramowicz M. A., Bulik T., Bursa M., Kluźniak W. 2003 *A&A*, 404, L21
- Abramowicz, M. A., Karas, V., Kluźniak, W., Lee, W.H., Rebusco, P. 2003, *PASJ*, 55, 467
- Balsara D. 1995, *J. Comp. Phys.*, 121, 357
- Blaes, O. 1987, *MNRAS*, 227, 975
- Daigne F., Mochkovitch R. 1997, *MNRAS*, 285, L15
- Daigne F., Font J.A. 2004, *MNRAS*, 349, 841
- Davies M.B., Benz W., Piran T., Thielemann F.K. 1994, *ApJ*, 431, 742
- Font J.A., Daigne F. 2002, *MNRAS*, 334, 383
- Fragile, P. C. 2005, to appear in the proceedings of the XXII Texas Symposium on Relativistic Astrophysics and Cosmology (astro-ph/0503305)
- Hjorth, J. et al. 2003, *Nature*, 423, 847
- Igumenshchev I., Chen X., Abramowicz, M. 1996, *MNRAS*, 278, 236
- Kato S., Fukue J., Mineshige S. 1998 *Black Hole Accretion Disks* Kyoto University Press, Japan.
- Kato S. 2001, *PASJ*, 53, 1
- Kluźniak W., Lee W. H. 1998, *ApJ*, 494, L53
- Kluźniak W., Abramowicz M. A., Kato S., Lee W. H., Stergioulas N. 2004, *ApJ*, 603, L89
- Kulkarni, S. et al. 1998, *Nature*, 395, 663
- Lee W. H. 2001, *MNRAS*, 328, 583
- Lee W. H., Ramirez-Ruiz E. 2002, *ApJ*, 577, 893
- Lee W. H., Abramowicz M., Kluźniak W. 2004, *ApJ*, 603, 93L
- McClintock, J. E., Remillard, R. 2004, in *Compact Stellar X-Ray Sources*, ed. W. H. G. Lewin & M. van der Klis (Cambridge: Cambridge Univ. Press), in press (astro-ph/0306213)
- Monaghan J. J. 1992, *ARA&A*, 30, 543
- Monaghan J. J., Lattanzio J. C. 1985, *A&A*, 149, 135
- Masuda N., Nishida S., Eriguchi Y. 1998, *MNRAS*, 297, 1139
- Michel F. 1972, *AP&SS*, 15, 153
- Montero, P., Rezzolla, L., Yoshida, S. 2004, *MNRAS*, 354, 1040
- Nomoto K., Maeda K., Mazzali P., Umeda H., Deng J., Iwamoto K. 2004, in *Stellar Collapse* edited by Chris L. Fryer, Astrophysics And Space Science Library Vol. 302, Kluwer Academic Publishers, The Netherlands.
- Ortega-Rodríguez, M., Silbergleit, A. S., Wagoner, R. V. 2002, *ApJ*, 567, 1043
- Paczynski B. 1998, *ApJ*, 494, L45
- Paczynski B., Wiita J. 1980, *A&A*, 88, 23
- Papaloizou J. C., Pringle J. E. 1984, *MNRAS*, 208, 31
- Perez, C. A., Silbergleit, A. S., Wagoner, R. V., Lehr, D. E. 1997, *ApJ*, 476, 589
- Rebusco P. 2004, *PASJ*, 56, 553
- Rezzolla L., Yoshida S., Maccarone T. J., Zanutti O. 2003, *MNRAS*, 344, L37
- Rezzolla L., Yoshida S., Zanutti O. 2003, *MNRAS*, 344, 978
- Rosswog, S., Speith, R., Wynn, G. A. 2004, *MNRAS*, 351, 1121
- Ruffert M., Janka H. Th. 1999, *A&A* 344, 573
- Ruffert M., Janka H. Th., Schaefer G. 1996, *A&A* 311, 352
- Rubio-Herrera E., Lee W. H. 2005, *MNRAS*, 357, L31
- Schnittman, J. D. 2005, *ApJ*, 621, 940
- Shapiro S., Shibata M. 2002, *ApJ*, 577, 904
- Shibata M., Shapiro S. 2002, *ApJ*, 572, L39
- Silbergleit, A. S., Wagoner, R. V., Ortega-Rodríguez, M. 2001, *ApJ*, 548, 335
- Stanek, K. et al. 2003, *ApJ*, 591, L17
- van der Klis, M. 2000, *ARA&A*, 38, 717
- van Putten M. H. P. M. 2001, *Phys. Rev. Lett.* 87, No. 9. (091101-1)
- Wagoner, R. V. 1999, *Phys. Rep.* 311, 259
- Wilson D.B. 1984, *Nature*, 312, 620
- Woosley S. E. 1993, *ApJ*. 405, 273
- Zanutti O., Rezzolla L., Font J. A. 2003, *MNRAS*, 341, 832
- Zanutti O., Font J. A., Rezzolla L., Montero P. J. 2005, *MNRAS*, 356, 1371
- Zurek W. H., Benz W. 1986, *ApJ*, 308, 123